I.K. Senchenkov, I.A. Ryabtsev, E. Turyk, O.P. Chervinko, I.I. Ryabtsev, A.A. Babynets

# Calculations of the Number of Allowed Surfacing-Based Repairs of Machinery Elements Exposed to Cyclic Thermal and Mechanical Loads

**Abstract:** The article presents a method enabling the assessment of fatigue service life and the calculation of the number of allowed surfacing-based repairs of cylindrical elements (on the side surface) exposed to thermal and mechanical service loads. A cylinder intended for hot operation was subjected to analysis aimed to determine the allowed number of surfacing-based repairs. As a result, it was possible to assess the entire duration of safe cylinder operation.

**Keywords:** fatigue service life, surfacing-based repairs, cylindrical elements

**DOI:** *10.17729/ebis.2017.6/3*

During their operation, hot rolling rollers, rolls used in continuous steel casting lines, moulds for hot stamping and some other surfaced machinery elements are exposed to cyclic thermal and mechanical stresses. At the first stage, cyclic thermal stresses are responsible for the formation of fatigue cracks (so-called annealing cracks) on the surface of the above-named elements. Such cracks are removed through machining, after which the elements are subjected to resurfacing. Afterwards, as fatigue failures accumulate, the aforesaid elements can be destroyed during operation, which could results in significant material losses.

This research work presents a method enabling the evaluation of fatigue service life and the allowed number of surfacing-based repairs of the lateral surface of cylindrical elements exposed to thermal and mechanical stresses.

The assessment of the stress-strain condition and microstructures of the above-named elements, their fatigue service life and the allowed number of surfacing-based repairs involves the numerical modelling of thermo-mechanical processes. The surfacing process consists in the application of molten metal on the surface of an element. In terms of the deformable solid mechanics, such processes are well described using non-classical models of the so-called accruing bodies [1]. In terms of surfacing and allied technologies, the aforementioned models are presented in works [2, 3].

The process of surfacing is performed within a wide range of homologous temperatures, where a material reveals thermo-plastic properties. Experimental and theoretical tests of such behaviour can be described using the co-called unified flow models based on the idea of

I.K. Senchenkov, Professor PhD (DSc) Habilitated; O.P. Chervinko PhD (DSC) – S. P. Timoszenko Mechanical Engineering Institute, the National Academy of Sciences of Ukraine, Kiev; I.A. Ryabtsev, Professor PhD (DSc) Habilitated Eng.; I.I. Ryabtsev, PhD (DSC); A.A. Babynets, PhD (DSC) – E. O. Paton Electric Welding Institute, the National Academy of Sciences of Ukraine, Kiev, Ukraine; dr hab inż. Eugeniusz Turyk (PhD (DSc) Habilitated Eng.) Professor Extraordinary at Instytut Spawalnictwa, Gliwice, Poland

internal state variables [4], e.g. the Bodner-Partom model [5], substantiated experimentally and sufficiently popular in practical applications, including those related to the process of surfacing [6, 7].

The solution to the problems addressed in works [2, 3] involved the development of a finite element methodology combined with implicit time increment schemes of the integration of non-stationary equations as well as iterative methods of the solving of non-linear boundary value problems of thermomechanics at each time increment. The present state of the numerical modelling of examined problems is presented in monographs [6, 8].

## Problem and the Adopted Model of Solution

The object subjected to the tests was a roller used in hot rolling processes (Fig. 1). The roller was made of steel 51CrMnV4, provided with the buffer zone surfaced using solid wire S1 according to EN ISO 14171 (equivalent of unalloyed steel DC01) and the external working layer surfaced using flux-cored wire PP-Np-25H5FMS (equivalent of tool steel 25Cr5VMoSi). The diameter of the roller barrel was 1435 mm.

After surfacing, the roller is subjected to service thermal and mechanical stresses. It is assumed that the roller is supported by a rigid backing roller and is not subjected to bending.

The problem of the girth helical surfacing and the subsequent cyclic loading of the roller is three-dimensional (3D problem). Taking into consideration the two stages of the process, i.e. surfacing and operation, as well as the axial extent of the roller geometry, the following approach to the problem is suggested:

1. The stage of surfacing is modelled within the axial-symmetric problem.
2. The stage of operation, characterised by highly located contact thermo-mechanical loads, is described within the problem concerning the flat strain in relation to the axial section of the roller A-A (Fig. 1).

The mode adopted when solving of the problem in relation to the stage of operation should take into consideration internal strains ($\varepsilon_{zz} \neq 0$) generated at the stage of surfacing. In this respect, the above-formulated problem differs from the classical flat strain-related problem, where longitudinal internal strains do not occur ($\varepsilon_{zz} = 0$).

The mechanical behaviour of the material can be described using the Bodner-Partom model containing the following dependences in the cylindrical coordinate system $Orz\varphi$ :

– flow rule with the condition of plastic incompressibility

$$\dot{\varepsilon}_{ij} = \dot{\varepsilon}^p_{ij} + \dot{\varepsilon}^e_{ij} \quad \dot{\varepsilon}^p_{kk} = 0,\ i, j = r, z, \varphi \tag{1}$$

– Prandtl-Reuss flow rule

$$\dot{\varepsilon}^p_{ij} = \frac{D_0}{J_2^{1/2}} \exp\left[ -\frac{1}{2}\left( \frac{K_0 + K}{\sqrt{3J_2}} \right)^{2n} \right] s_{ij} \tag{2}$$

where $J_2 = \frac{1}{2} s_{ij} s_{ij}$ ; $s_{ij} = \sigma_{ij} - \frac{1}{3}\delta_{ij}\sigma_{kk}$ ;

– equation of evolution in relation to the parameter of isotropic hardening $K$

$$\dot{K} = m_1 (K_1 - K)\dot{W}_p,\ K(0) = 0 \tag{3}$$

where $\dot{W}_p = \sigma_{ij}\dot{\varepsilon}^p_{ij}$ ; $D_0$, $K_0$, $K_1$, $m_1$, $n$ – model parameters,

– Hooke's law

$$\sigma_{kk} = 3K_v(\varepsilon_{kk} - 3\alpha(\theta - \theta_0)),\ s_{ij} = 2G\left(e_{ij} - \varepsilon^p_{ij}\right),$$
$$e_{ij} = \varepsilon_{ij} - \tfrac{1}{3}\varepsilon_{kk}\delta_{ij} \tag{4}$$

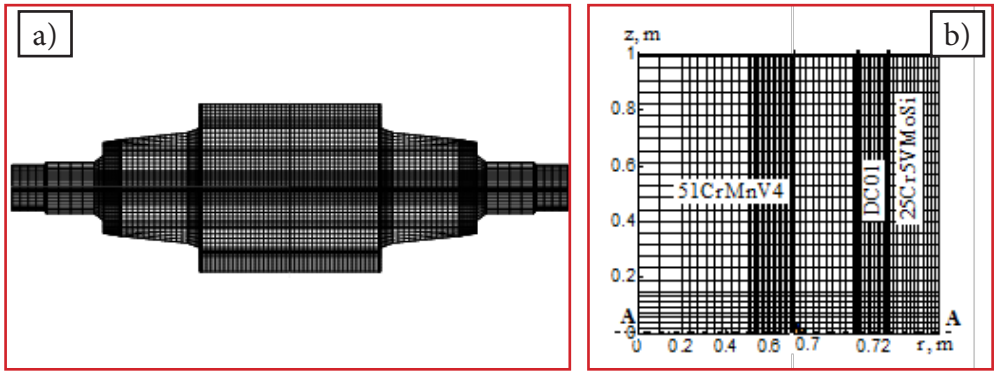


Fig. 1. Mesh of finite elements of the roller (a) and its surfaced barrel (b)

where $G$, $K_V$, $\alpha$ – modules of transverse elasticity, volumetric elastic compressibility and the coefficient of linear expansion.

The dependences supplement the universal equation of the pseudo-static equilibrium and thermal conductivity in relation to the axial-symmetric problem:

$$\frac{\partial \sigma_{rr}}{\partial r}+\frac{1}{r}\left(\sigma_{rr}-\sigma_{\varphi\varphi}\right)+\frac{\partial \sigma_{rz}}{\partial z}=0,\quad \frac{\partial \sigma_{rz}}{\partial r}+\frac{1}{r}\sigma_{rz}+\frac{\partial \sigma_{zz}}{\partial z}=0, \tag{5}$$

$$c_V\dot{\theta}=\frac{1}{r}\frac{\partial}{\partial r}\left(\lambda\frac{\partial \theta}{\partial r}\right)-\frac{\partial}{\partial z}\left(\lambda\frac{\partial \theta}{\partial z}\right)+Q \tag{6}$$

where $c_v$ and $\lambda$ – specific heat referred to the volume unit and the thermal conductivity coefficient, $Q$ – power of the volumetric heat source, $\dot{\theta}=\partial\theta/\partial t$, as well as the boundary and initial conditions (in relation to temperature):

$$\sigma_{rr}=\sigma_{rz}=0,\quad -\lambda\frac{\partial \theta}{\partial r}=\alpha\left(\theta-\theta_c\right)+cc_0\left(T^4-T_c^4\right),$$
$$r=R,\ R+h,\ 0<z<l,\ t\neq t_{1,2}^{*}; \tag{7}$$

$$\sigma_{zz}=\sigma_{rz}=0,\quad \pm\lambda\frac{\partial \theta}{\partial r}=\alpha\left(\theta-\theta_c\right)+cc_0\left(T^4-T_c^4\right),$$
$$z=0,\ r=R,R+\tilde{h},\ t>0; \tag{8}$$
$$\theta=\theta_c;\ t=0$$

where $\tilde{h}=h_1,\ h_1+h_2$ – thickness of layers changing during the process of surfacing; $h_1$, $h_2$ – thickness of the first and second surfaced layer, $t_{1,2}^{*}$ – time of application of surfaced layers; $c$ – relative emissivity; $c_0$ – Stefan-Boltzman constant; $\alpha$ – convective heat transfer coefficient; $\theta_c$ – ambient temperature.

The process of surfacing is considered within the model of accruing bodies, developed in works [2, 3, 7] using the idea of internal stresses and temperature.

To allow for phase transformations in the materials, the calculations concerning phase contents were performed on the basis of austenite transformation diagrams in relation to steel 51CrMnV4 and 25Cr5VMoSi [9]. The aforesaid diagrams present transformations in steel during cooling, related to the decomposition of austenite ($\xi = A$) as well as the formation of ferrite ($\xi = F$), pearlite ($\xi = P$), bainite ($\xi = B$) and martensite ($\xi = M$). The law of the accumulation of new phase $\xi$ in appropriate areas along the curve of cooling is defined by the Koistinen-Marburger phenomenological equation [10].

Properties of each phase $Y_\xi$ are calculated allowing for their dependence on temperature $Y_\xi = Y_\xi(\theta)$. Calculations of macro-characteristics $Y$ in relation to any phase composition involve the use of the linear mixture rule. The general formula has the following form:

$$Y\left(\theta,t\right)=\sum_{\xi}C_\xi\left(\theta,t\right)Y_\xi\left(\theta\right) \tag{9}$$

Physical quantities calculated according to the mixture rule can include $c_v$ – specific heat, $k$ – heat conductivity coefficient, $E$ – Young's modulus, $\alpha$ – linear expansion coefficient, $\nu$ – Poisson constant. Within a wide range of temperatures, the mixture rule is applied and compared with experiments described in works [2, 8].

Fatigue service life is evaluated using the Manson-Birger model [11]. If the load cycle is asymmetric and the Goodman equation is taken into consideration the following formula [12] is obtained:

$$\Delta\varepsilon=\left(\ell n\frac{1}{1-\psi}\right)^{0,6}N^{-0,6}+\frac{2\sigma_{-1}}{E}\left(1-\frac{\sigma_m}{\sigma_B}\right)\left(\frac{N}{N_0}\right)^{k} \tag{10}$$

where $\sigma_{-1}$ – ultimate fatigue strength, $N_0$ – ultimate number of cycles, $\Psi$ – plasticity at fracture, $k$ – parameter defining the inclination angle of the fatigue curve, $\sigma_B$ – tensile strength, $\sigma_M$ and $\sigma_a$ – mean and amplitude cycle stress.

If the cyclic plastic strain is not present $\Delta\varepsilon^p = 0$, the first component in (10) can be omitted. As a result, taking into consideration the dependence $\Delta\varepsilon = \Delta\sigma / E$, $\Delta\sigma = 2\sigma_a$, the following is obtained:

$$\ell gN=\frac{1}{k}\ell g\left[\frac{\sigma_{-1}}{\sigma_B}\left(\frac{\sigma_B-\sigma_m}{\sigma_a}\right)N_0^{k}\right] \tag{11}$$

Moving from the uniaxial equation (11) the multiaxial strain condition is performed using the equivalent stress $\sigma_i=\sqrt{3}s_i=\left(2/3\,s_{ij}s_{ij}\right)^{1/2}$ [11].

After transformations, taking into consideration dependences $\sigma_{ia} = \sqrt{3}s_{ia}$ and $\sigma_m = \sqrt{3}s_{im}$, the following equation is obtained:

$$\ell gN = \frac{1}{k}\ell g\left[\chi\left(\frac{\sigma_B - \sqrt{3}s_{im}}{s_{ia}}\right)\right] \quad (12)$$

where

$$\chi = \frac{\sigma_{-1}}{\sigma_B}\frac{N_0^k}{\sqrt{3}} \quad (13)$$

Values of quantities $\sigma_B = \sigma_B(\theta)$, $\sigma_{-1} = \sigma_{-1}(\theta)$, $N_0$ $(\theta)$ and $k$ $(\theta)$ in relation to each material were adopted according to publication [12], whereas values $s_{ia}$, $s_{im}$ and $\theta$ were calculated at each point of the roller using numerical methods.

The instantation of dependence (12) required the use of the following simplifying assumptions: dependence $\sigma_{-1}$ $(\theta)$ / $\sigma_B$ $(\theta)$ = *const*, $k$ = *const* and $N_0$ = *const* in relation to all temperatures, tensile strength $\sigma_B$ depended on temperature and, in dependence (12), was calculated in relation to the maximum value of temperature in the cycle.

As a result, the following equations of fatigue curves allowing for temperature and the mean stress were obtained:

– for steel S1

$$\ell gN = 4{,}35\ell g\left[7{,}17\left(\frac{\sigma_B(\theta) - \sqrt{3}s_{im}}{s_{ia}}\right)\right] \quad (14)$$

– for steel 25Cr5VMoSi

$$\ell gN = 7{,}35\ell g\left[1{,}54\left(\frac{\sigma_B(\theta) - \sqrt{3}s_{im}}{s_{ia}}\right)\right] \quad (15)$$

– for steel 51CrMnV4

$$\ell gN = 12{,}8\ell g\left[2{,}064\left(\frac{\sigma_B(\theta) - \sqrt{3}s_{im}}{s_{ia}}\right)\right] \quad (16)$$

The problem of the service load of the roller was formulated within the confines of the flat strain in relation to the middle cross-section $z = L/2$. In the polar coordinate system $Or\varphi$, the typical distribution of temperature in the development $\varphi^* = \varphi - \omega t$, where $\omega$ – angular frequency of the rotation of the roller, is presented in Figure 2.

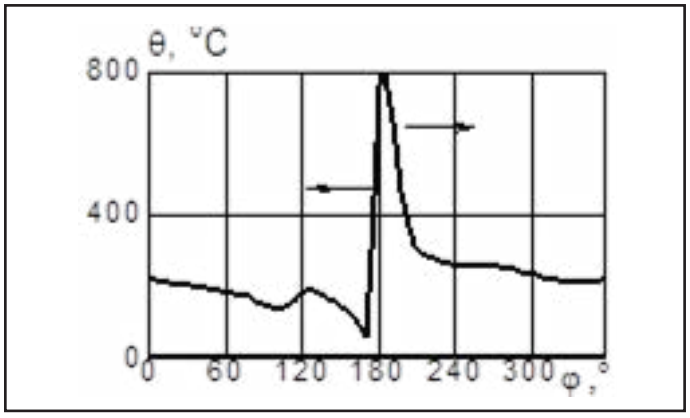


Fig. 2. Distribution of temperature on the surface of the roller during its rotation by angle $\varphi$

In the contact area between the roller and a heated metal subjected to rolling the adopted boundary conditions have the following form:

$$\sigma_{rr} = \sigma(\varphi^*),\ \sigma_{rz}(\varphi^*) = 0,\ |\varphi^*| < \varphi_0{}^* \quad (17)$$

where $\varphi^* = \varphi - \omega t$ ;

For $\sigma(\varphi^*)$, the Hertz distribution of contact stresses [13] $\sigma(\varphi*) = p_0\sqrt{1-\left(\varphi^*/\varphi_0^*\right)^2}$ is used, where $2\varphi_0{}^*$ – load-affected area.

## Calculations of Internal Stresses

The calculations involved the simplified scheme of the immediate surfacing of successive layers. The surface of the roller face during the surfacing of the buffer layer having thickness $h_1$ = 5 mm reaches a temperature of 1800°C after 2.8 seconds. Once the element has cooled down to 300°C, its surface is reheated and reaches a temperature of 1800°C after 2.8 seconds during the surfacing of the working layer. Afterwards the element cools down to an ambient temperature of 20°C.

The volumetric content of the structures as well as the stress-strain condition of the element subjected to surfacing are presented in Figure 3. The bold full lines depict layer boundaries. The structure of the working layer is mostly martensitic, whereas that of the heat affected zone is mostly bainitic. The martensitic phase is characterised by the greatest volume, therefore the internal stresses in the working layer are compressive, whereas those in the buffer layer and in the base material are tensile (Fig. 3b).

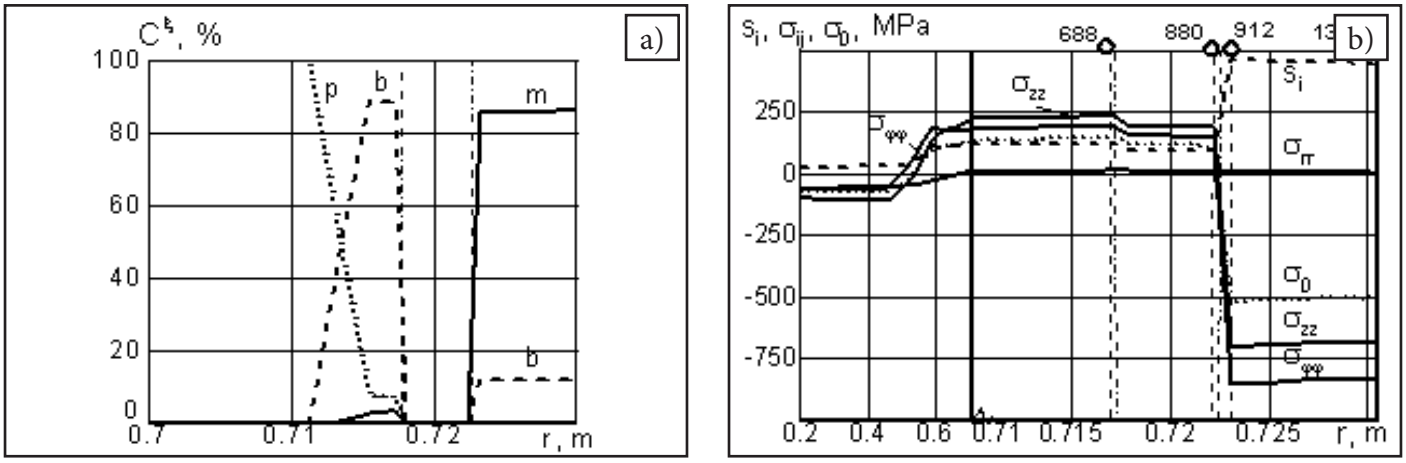


Fig. 3. Structural contents (a) and the stress-strain condition (b) of the surfaced roller: 1 – base material, 2 – buffer layer, 3 – working layer, p – pearlite, b – bainite, f – ferrite, m – martensite. Numbers in the upper fragment of Figure 3 correspond to the numbers of points in Figure 4b; $\sigma_0 = 1/3\sigma_{kk}$

## Calculations of Service Stresses

Figure 4a presents the finite element mesh related to the cross-section of the roller $z = L/2$ (cross-section A-A in Figure 1); Figure 4b presents the fragment of the mesh marked using the dashed line in Figure 4a. Numbers in the above-named figure and in Figure 3 signify the numbers of the nodes, in relation to which the indicators of the stress-strain condition were calculated. Arrows indicate areas where moving loads were applied, $v$ – linear velocity of the surface points (rolling rate). The dashed lines in Figure 4b signify layer boundaries.

Time dependences related to components of stresses and temperature in relation to point 1360 near the roller surface for $v$ = 0,5 m/s are presented in Figure 5a. As can be seen, in the area of contact with the hot rolled metal ($\theta = \theta_{max}$), stresses in the surface layer are compressive. During cooling the above-named stresses become tensile. The calculations revealed that in relation to $p_0 < 300$ Mpa, the effect of mechanical components of the load is negligible and that the stress-strain condition (SSC) is affected by the thermal load.

## Service Life Assessment

Service life was calculated, using formulas (14)÷(16), in relation to each point of the roller cross-section (Fig. 4b). Figure 5 presents the exemplary radial distribution of service life $lgN$ as well as the mean $s_{im}$ and amplitude values of the intensity of stresses $s_i$ in relation to cycle $p_0 = 0$, $\theta_{max} = 500°C$ .

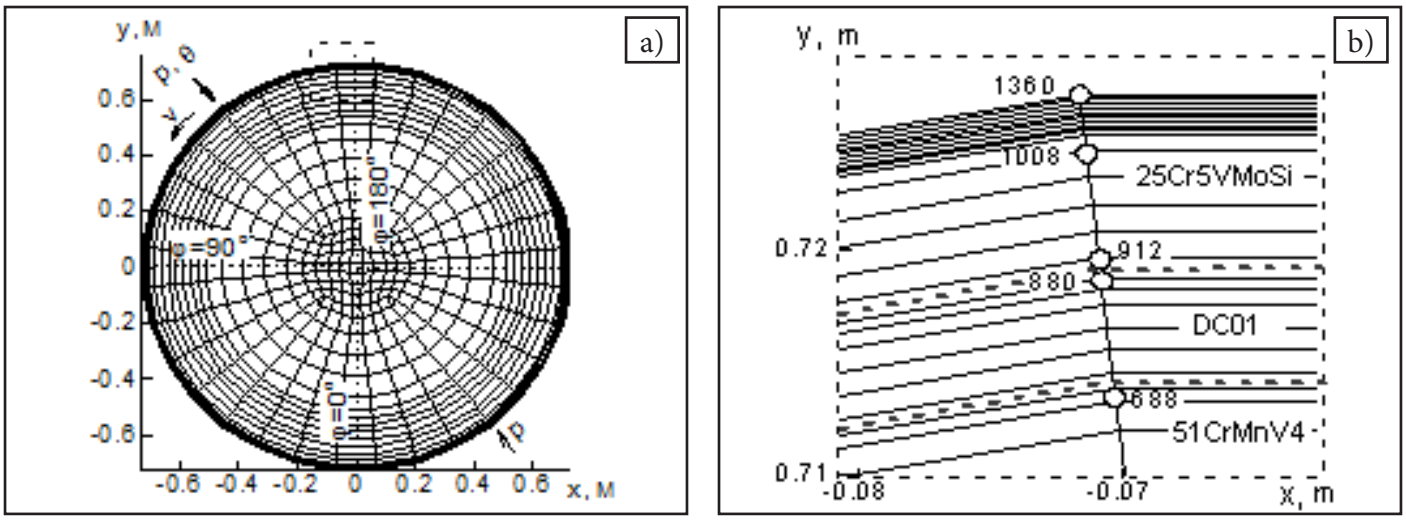


Fig. 4. Finite element mesh and the schematic diagram of the operational load of the roller: a – entire cross-section, b – sector of the mesh and numbers of points

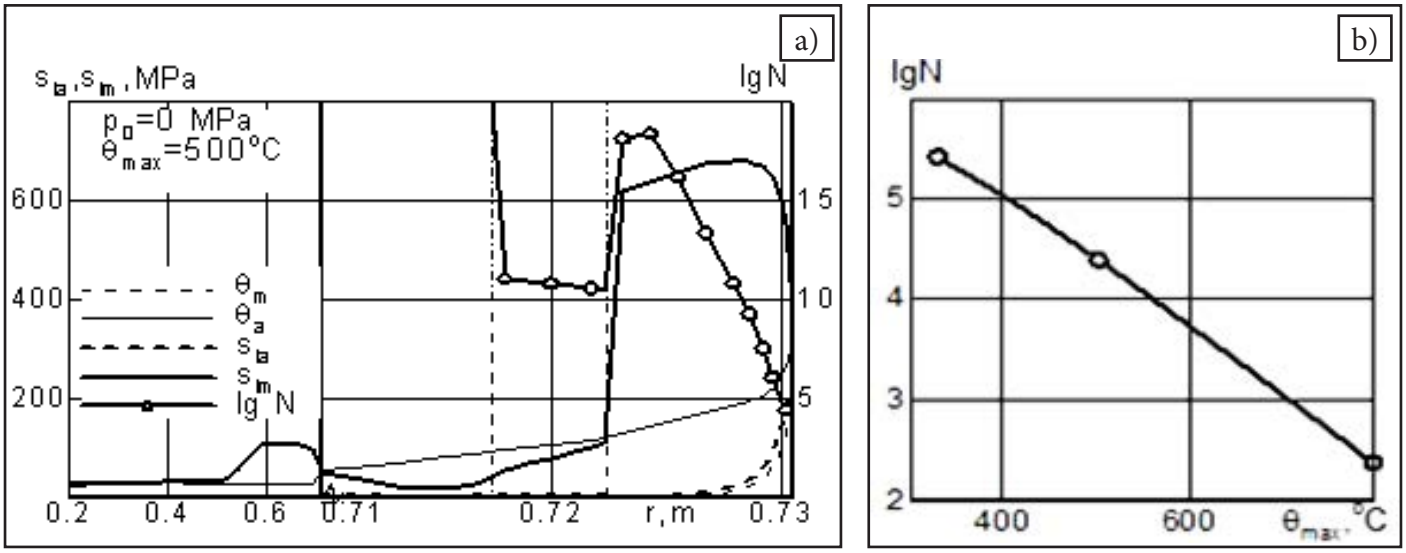


Fig. 5. Radial distribution of service life lg $N$, mean $s_{im}$ and amplitude $s_{ia}$ values of the intensity of stresses $s_i$ in relation to cycle $p_0 = 0$, $\theta_{max} = 500$°C (a) as well as the dependence of the working layer on temperature (b); 1 – base material, 2 – buffer layer, 3 – working layer

Table 1. Fatigue service life *lgN* of the layer surfaced using wire 25Cr5VMoSi

| $\theta_{max}$, °C | Service life *lgN* in relation to | | | | | |
|---|---|---|---|---|---|---|
| | $p_0$ = 0 MPa | | $p_0$ = 200 MPa | | $p_0$ = 1000 MPa | |
| | without buffer layer | buffer layer S1 | without buffer layer | buffer layer S1 | without buffer layer | buffer layer S1 |
| 20 | - | - | 12.33 | 12.51 | 6.05 | 6.35 |
| 570 | 5.34 | 5.50 | 5.10 | 5.45 | 5.20 | 5.35 |
| 860 | 3.34 | 3.90 | 3.45 | 3.75 | 3.52 | 3.79 |

As can be seen, the minimum service life $N \approx 10^4$ is that of the surface layers of the outer surfaced layer (working layer). The service life of the surface layer significantly depends on temperature (Fig. 5b). In the above-presented conditions, the buffer layer and the base material are characterised by significantly higher service life.

The comparison of the calculation results concerning the fatigue service life is presented in Tables 1 and 2. As can be seen from the results presented in Table 1, nearly in all of the cases the surfacing of the buffer layers increased the fatigue service life of the surfaced working layer (25Cr5VMoSi).

Table 2. Fatigue service life *lgN* of the buffer layer surfaced using wire S1

| $\theta_{max}$, °C | Service life *lgN* in relation to | | |
|---|---|---|---|
| | $p_0$ = 0 MPa | $p_0$ = 200 MPa | $p_0$ = 1000 MPa |
| 20 | - | 10.80 | 7.96 |
| 570 | 7.09 | 5.62 | 3.80 |
| 860 | 6.45 | 5.58 | 3.72 |

## Scheme of Repeated Repair Surfacing

The calculations revealed that in terms of the predominantly thermal load cycle the service life of the buffer zone ( $N_{f_2}$ ) was significantly higher than that of the outer layer ( $N_{f_1}$ ). It was also revealed that the service life of the base material ( $N_{f_3}$ ) was significantly higher than that of the surfaced layers $N_{f_3} > N_{f_1} > N_{f_2}$. The proportion of parameters $N_{f_1}$, $N_{f_2}$, $N_{f_3}$ determines repair schemes 1, 2 and 3:

– repair according to scheme 1 comes down to the removal of the damaged outer heat–resistant layer followed by the surfacing of this layer. The scheme is used to perform $k_1$ repairs, determined by the following condition:

$$k_1 N_{f_1} = N_{f_2} \tag{18}$$

– satisfaction of condition (18) is followed by the repair performed according to scheme 2, where both the outer working layer and the buffer layer are removed and resurfaced; repairs according to scheme 1 and 2 are performed until the satisfaction of the following condition:

$$k_2 N_{f_2} = N_{f_3} \quad (19)$$

where $k_2$ – number of repairs according to scheme 2;

– satisfaction of condition (19) is followed by the repair according to scheme 3, involving the removal and the resurfacing of both layers and of the damaged base material layer.

Calculations concerning preventive surfacing processes, operating thermo-mechanical cycles and repair welding are extensive. For this reason it is important to answer the question where the internal stress-strain condition (SSC) in the layers and in the base material after repair surfacing cycles performed according to schemes 1, 2 and 3 is restored and whether the SSC cycles are stable when exposed to the service load.

It should be noted that correlations (18) and (19) are correct provided that residual stresses are restored without visible changes in the surfacing cycle according to scheme 1 and 2. The justification of the above-presented assumption involved the performance of the numerical modelling of repair surfacing processes in accordance with the schemes illustrated with the example of the two-layer surfacing involving the lateral surface of the roller, i.e. the buffer zone surfaced using wire S1 and the outer layer:

1. Preventive surfacing 0.
2. Thermo-mechanical cyclic load having parameters $\theta_{max}$ = 570°C, $\theta_{min}$ = 60°C, $p_0$ = 500 MPa, until the obtainment of the cyclic stability of the SSC (3 cycles).
3. After cooling to $\theta_{min}$ = 50°C, the removal of the outer layer.
4. Surfacing 1.
5. Thermo-mechanical cyclic load having parameters $\theta_{max}$ = 570°C, $\theta_{min}$ = 60°C, $p_0$ = 500 MPa, until the obtainment of the cyclic stability of the SSC.
6. After cooling to $\theta_{min}$ = 50°C, the removal of the outer layer.
7. Surfacing 2.

The calculation results are illustrated in Figure 6 using the axial distributions of the intensity of contact stresses $s_i$.

As can be seen, the stress intensity responsible for service life is well restored after each repair surfacing according to scheme 1, where «surfacing 0» corresponds to the preventive surfacing performed during the production of the roller.

The assessment of the stability of internal SSC during repair surfacing according to scheme 2 was performed on the basis of the two-layer surfacing involving the lateral surface of the roller, composed of the buffer zone surfaced using wire S1 and of the outer layer. The roller was subjected to the following procedures:

1. Preventive surfacing 0.
2. Thermo-mechanical cyclic load having parameters $\theta_{max}$ = 570°C, $\theta_{min}$ = 60°C, $p_0$ = 500 MPa, until the obtainment of the cyclic stability of the SSC (3 cycles).
3. After cooling to $\theta_{min}$ = 50°C, the removal of two layers.
4. Two-layer repair surfacing.

The calculation results present axial distributions related to the intensity of contact stresses

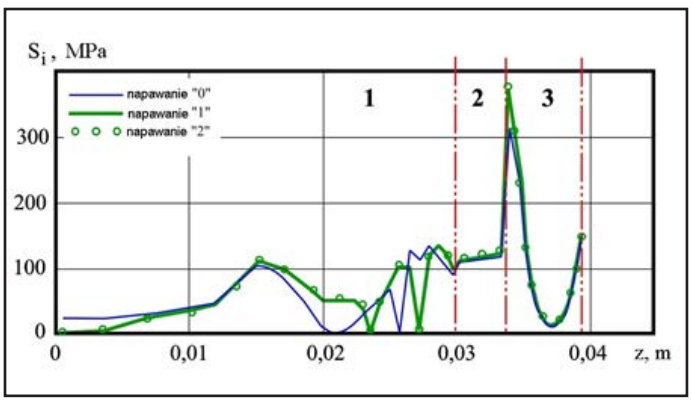


Fig. 6. Comparison of axial distributions related to the intensity of stresses $s_i$ after preventive surfacing "0" and surfacing "1": 1 – base material, 2 – surfaced buffer layer, 3 – surfaced layer resistant to wear; scheme 1

(Fig. 7). Also in this case, similar to surfacing according to scheme 1 (Fig. 6), parameter is well restored after each repair surfacing according to scheme 2.

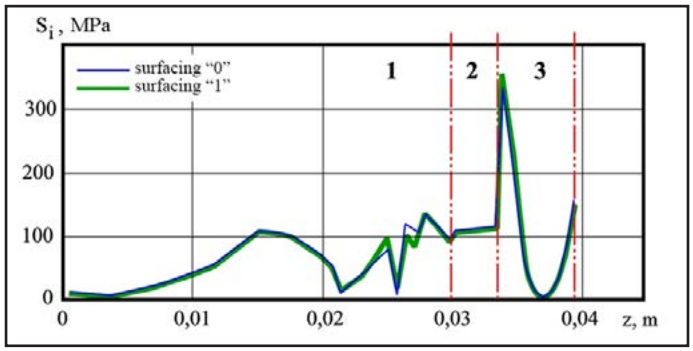


Fig. 7. Comparison of axial distributions related to the intensity of stresses $s_i$ after preventive surfacing "0" and surfacing "1": 1 – base material, 2 – surfaced buffer layer, 3 – surfaced layer resistant to wear; scheme 2

In general, the entire scheme of repeated repair surfacing is presented in Figure 8, where WL – fragment related to the work layer, BL – fragment related to the buffer layer and BM – fragment related to the base material, $\omega_i$ – susceptibility of the structural element to failure $\omega_i = N_f / N_{f_i},\ i = 1,\ 2,\ 3$.

Because of the fact that susceptibility to failures is of random nature, it is necessary to define the repair-related values of operation cycles:

$$N_{1p} = \alpha_1 N_{f_1},\ N_{2p} = \alpha_2 N_{f_2},\ N_{3p} = \alpha_3 N_{f_3} \qquad (20)$$

where $\alpha_1$, $\alpha_2$, $\alpha_3$ – margin coefficient, $0 < \alpha_{1,2,3} < 1$.

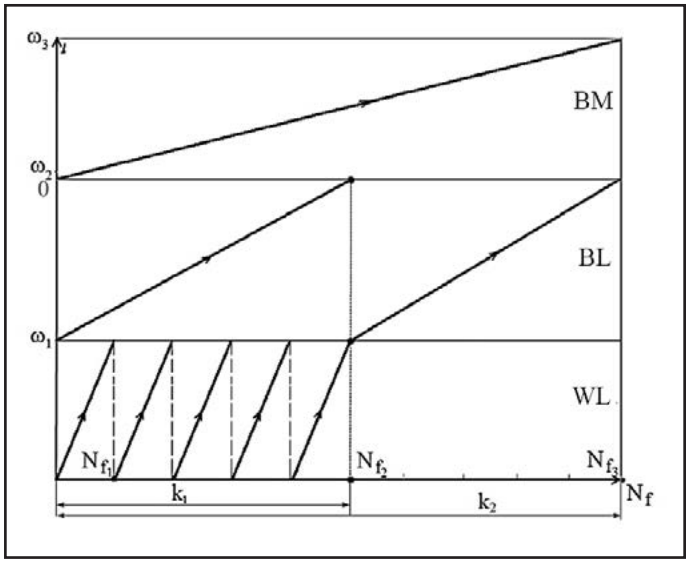


Fig. 8. Scheme of repeated repair surfacing (designations as in the text)

Then, it is possible to formulate more conservative assessments of repair conditions:

$$k_1 N_{f_{1p}} = N_{2p},\ k_2 N_{f_{2p}} = N_{3p} \qquad (21)$$

The above-presented scheme can be treated as "regular". It corresponds to the service life combined with the formation of a "small" crack $l \approx 1 \div 2$ mm related to a fatigue crack. The scheme requires generalisation in the event of the development of another micro-crack passing through surfaced layers and, possibly, reaching the base material. The higher the heterogeneity of the material and the greater the number of micro-imperfections, the lower the values determined in relation to margin coefficients $\alpha_{1,2,3}$. Calculations of repair cycles should include values $N_{f_1}$, $N_{f_2}$, $N_{f_3}$, at the most exposed (loaded) points of surfaced layers and of the base material. The presented scheme can be generalised in relation to any number of surfaced layers.

The exemplary calculation is concerned with the number of allowed repairs in relation to the surfacing of the specimen provided with the buffer layer made using wire S1, where values of loads are similar to those occurring in actual operating conditions (60°C < $\theta$ < 860°C, $p_0$ = 200 MPa). Initial data include data concerning the service life of the buffer layer and the layer resistant to wear in relation to the loads presented in Tables 1 and 2.

$lgN_{f_1} = 3.75;\ lgN_{f_2} = 5.58$ or $N_{f_1} = 5.6 \cdot 10^3;\ N_{f_2} = 3.3 \cdot 10^5$.

According to Manson [11], the margin for the random nature of fatigue crack formation in engineering practice amounts to one decade. As a result, it is assumed that $\alpha_1 = 10^{-1}$; $\alpha_2 = 10^{-2}$. Adopted value $\alpha_2$ is by one order lower than $\alpha_1$ as the buffer layer operation time and, consequently, the probability of crack development significantly exceed those of the outer layer. Taking into consideration the above named factors and correlations (20), the following (in relation to the thermo-mechanical cycle) is obtained:

$N_{1p} \approx 6 \cdot 10^2$; $N_{2p} \approx 3 \cdot 10^3$,

hence in accordance with (21): $k_1 \approx 5$.

Therefore, in cases of cyclic thermal and mechanical loads similar to actual operating conditions it is allowed to perform not more than five repairs according to scheme 1, where, to exclude the likelihood of fatigue failure, it is necessary to remove and re-resurface both the working and buffer layer.

## Conclusions

1. The research-related work and tests resulted in the development of a methodology enabling the performance of the mathematical modelling of the process covering the entire "life history" of machinery elements, including preventive surfacing performed when manufacturing a new element, the period of operation and the multiple (repeated) multilayer repair surfacing according to three different schemes.

2. The example of the surfaced roller (used for hot rolling) subjected to a thermo-mechanical load cycle was used to justify schemes applied for the repeated repair surfacing of the above-named roller as well as to determine the allowed number of surfacing-based repairs enabling the assessment of the entire safe service life of the roller.

## References


[1] Арутюнян Н.Х., Дроздов А.Д., Наумов В.Э.: *Механика растущих вязкоупругопластических тел*. Изд. Наука, Москва, 1987. p. 472

[2] Senchenkov I.K., Chervinko O.P., Banyas M.V.: *Modeling of thermomechanical process in growing viscoplastic bodies with accounting of microctructural transformation*. In: R.B. Hetnarski (ed.). Encyclopedia of Thermal Stresses. Springer, 2014, vol. 6, pp. 3147–3157. http://dx.doi.org/10.1007/978-94-007-2739-7_618

[3] Senchenkov I.K., Chervinko O.P., Turyk E., I.A. Ryabtsev I.A.: *Examination of the thermomechanical state of cylindrical components deposed with layers of austenitic and martensitic steels.* Welding International, 2008, vol. 22, no. 7, pp. 457–464. http://dx.doi.org/10.1080/09507110802352340

[4] Krempl E.: *Viscoplastic models for high temperature applications.* International Journal of Solids and Structures. 2000, vol. 37, pp. 279 – 291. http://dx.doi.org/10.1016/s0020-7683(99)00093-1

[5] Bodner S.R.: *Unified Plasticity – An Engineering Approach (Final Report)*. Technion - Israel Institute of Technology, Faculty of Mechanical Engineering. Haifa, 2000, p. 106

[6] Рябцев И.А., Сенченков И.К., Турык Э.В.: *Наплавка. Материалы, технологии, математическое моделирование*. Wydawnictwo Politechniki Śląskiej, Gliwice, 2015, p. 590

[7] Сенченков И.К., Червинко О.П., Доля Е.В.: *Моделирование остаточного напряженно-деформированного и микроструктурного состояния цилиндра при наращивании по боковой поверхности слоями расплавленного металла*. Теоретическая и прикладная механика, 2014, Вып. 8 (54), pp. 34-44.

[8] Махненко В.И.: *Ресурс безопасности эксплуатации сварных соединений и узлов современных конструкций*. Изд. Наукова думка, Киев, 2006, p. 618

[9] Попов А.А. Попова Л.Е.: *Справочник термиста. Изотермические и термокинетические диаграммы распада переохлажденного аустенита*. ГНТИ Машиностр. лит., Москва, 1961, p. 430

[10] Koistinen D.R., Marburger R.E.: *A general equation prescribing the extent of austenite-martensite transformation in pure*

*iron-carbon alloys and carbon steel*. Acta Metallurgica, 1959, vol. 7, pp. 56-60. http://dx.doi.org/10.1016/0001-6160(59)90170-1

[11] Дульнев П.А., Котов П.И.: *Термическая усталость металлов*. Изд. Машиностроение, Москва, 1980, p. 200

[12] Трощенко Б.Т., Сосновский Л.А.: *Сопротивление усталости металлов и сплавов. Справочник*. Ч. 1. Изд. Наукова думка, Киев, 1987, p. 506

[13] Джонсон К.: *Механика контактного взаимодействия*. Изд. Мир, Москва, 1989, p. 510